Biochimica et Biophysica Acta 1778 (2008) 2765–2774

Contents lists available at ScienceDirect

Biochimica et Biophysica Acta

journal homepage: www.elsevier.com/locate/bbamem

Membrane insertion of the three main membranotropic sequences from SARS-CoV S2 glycoprotein

Jaime Guillén [a], Paavo K.J. Kinnunen [b], José Villalaín [a,*]

[a] Instituto de Biología Molecular y Celular, Campus de Elche, Universidad "Miguel Hernández", E-03202 Elche-Alicante, Spain
[b] Helsinki Biophysics and Biomembrane Group, Institute of Biomedicine/Medical Biochemistry, P.O. Box 63 (Haartmaninkatu 8), FIN-00014 University of Helsinki, Helsinki, Finland

ARTICLE INFO

Article history:
Received 26 May 2008
Received in revised form 9 July 2008
Accepted 23 July 2008
Available online 5 August 2008

Keywords:
SARS
Membrane fusion
Spike glycoprotein
Peptide–membrane interaction
Virus–host cell interactions
Lipid bilayers

ABSTRACT

In order to complete the fusion process of SARS-CoV virus, several regions of the S2 virus envelope glycoprotein are necessary. Recent studies have identified three membrane-active regions in the S2 domain of SARS-CoV glycoprotein, one situated downstream of the minimum furin cleavage, which is considered the fusion peptide ($SARS_{FP}$), an internal fusion peptide located immediately upstream of the HR1 region ($SARS_{IFP}$) and the pre-transmembrane domain ($SARS_{PTM}$). We have explored the capacity of these selected membrane-interacting regions of the S2 SARS-CoV fusion protein, alone or in equimolar mixtures, to insert into the membrane as well as to perturb the dipole potential of the bilayer. We show that the three peptides interact with lipid membranes depending on lipid composition and experiments using equimolar mixtures of these peptides show that different segments of the protein may act in a synergistic way suggesting that several membrane-active regions could participate in the fusion process of the SARS-CoV.

1. Introduction

Coronaviruses are a diverse group of enveloped, positive-stranded RNA viruses that cause respiratory and enteric diseases in humans and other animals. Severe acute respiratory syndrome coronavirus (SARS-CoV) is a newly emergent member in the family *Coronaviridae* that cause a severe infectious respiratory disease. SARS-CoV is distinct from previously characterized groups of coronaviruses [1,2], and unlike other human coronaviruses whose infections are usually very mild, SARS-CoV produced mortality rates as high as 10% but increased to greater than 50% in persons older than age 60 [3]. At present there is no vaccine available against any human coronavirus infection, and although SARS-CoV has been successfully restrained, re-emergence from animal reservoirs is still a potential risk for future recurrences [4].

SARS-CoV infection, similarly to other envelope viruses, is achieved through fusion of the lipid bilayer of the viral envelope with the host cell membrane [5,6], although recent studies have shown that the entry may be also pH-dependent [7]. The spike glycoprotein S is a surface class I viral fusion glycoprotein that mediates viral entry by binding to the cellular receptor and induces membrane fusion. The S1 subunit contains the receptor binding domain, whereas the S2 is responsible for the fusion between the viral and cellular membranes [2,8]. S2 contains two highly conserved heptad repeat regions (HR1 and HR2, see Fig. 1A) [9–11], similarly to other viral Class I fusion proteins, including HIV-1 gp41, influenza hemagglutinin HA2, Ebola virus glycoprotein and paramyxovirus F protein [12,13]. All of them have been classified as Class I transmembrane glycoproteins and are displayed on the surface of the viral membrane as oligomers. Class I viral proteins also contain a hydrophobic region denominated as the fusion peptide (FP) and other hydrophobic region immediately adjacent to the membrane-spanning domain denominated as the pre-transmembrane domain (PTM). Computer sequence predictions and systematic amino acid mapping studies of the S2 domain have located the HR1 region to amino acids approximately from 892 to 972, while the HR2 region extends approximately from amino acids 1142 to 1184 [2,10,11,14–17]. Binding of the S1 subunit to the receptor is thought to trigger a series of conformational changes in S2 that brings, via the formation of an antiparallel heterotrimeric six-helix bundle by the two HR regions, the putative fusion peptide and the transmembrane domain in close proximity. These structural rearrangements in the S protein generate the energy that drives the fusion of the viral and cellular lipid membrane.

Although it was initially believed that viral fusion glycoproteins interacted with the membrane solely by means of the FP, different

Abbreviations: CHOL, Cholesterol; CoV, Coronavirus; di-8-ANEPPS, 4-(2-(6-(Diocty-lamino)-2-naphthalenyl)-(ethenyl)-1-(3-sulfopropyl)-pyridinium inner salt; ESM, Egg sphingomyelin; FP, Fusion peptide; HR, Heptad repeat region; LUV, Large unilamellar vesicles; POPC, 1-Palmitoyl-2-oleoyl-*sn*-glycero-3-phosphocholine; POPG, 1-Palmitoyl-2-oleoyl-*sn*-glycero-3-phosphoglycerol; PTM, Pre-transmembrane domain; SARS, Severe acute respiratory syndrome; $SARS_{IFP}$, SARS internal fusion peptide; $SARS_{FP}$, SARS putative fusion peptide; $SARS_{PTM}$, SARS pre-transmembrane peptide; T_m, Temperature of the gel-to-liquid crystalline phase transition

* Corresponding author. Tel.: +34 966 658 762; fax: +34 966 658 758.
E-mail address: jvillalain@umh.es (J. Villalaín).

0005-2736/$ – see front matter © 2008 Elsevier B.V. All rights reserved.
doi:10.1016/j.bbamem.2008.07.021

regions of the viral envelope glycoproteins are essential for membrane fusion to occur [18–24]. These membrane-interacting regions are capable of modifying the biophysical properties of phospholipid membranes, suggesting that several segments may have an important role in the fusion process [18,25–31]. While much progress has been made in understanding the implication of fusion peptides of influenza, HIV and other viruses in fusion, available data concerning the fusion peptide of coronaviruses, particularly in the case of SARS-CoV, are scarce. It has been predicted that the sequence comprising residues from 858 to 886 of the S2 domain of the SARS-CoV spike glycoprotein is the FP domain since it has strong membrane-perturbing capacities [14,32], and furthermore mutations in this region cause inhibition of S-mediated cell fusion by more than 70% [33]. However, recent studies have shown that the region comprising residues 770 to 788 has a much more potent fusogenic activity than the former sequence and suggested to constitute the fusion peptide of the S2 glycoprotein [34]. The importance of PTM segments on the mechanism of viral entry has also been demonstrated in the membrane fusion proteins of HIV, FIV, Ebola virus, HSV and VSV through the use of site-directed mutagenesis and the study of the interaction of synthetic peptides with membranes [24,35–43]. Similar observations suggest that the PTM domain of SARS-CoV may also play an essential role in virus entry [32,44–46]. Upon triggering, the N-terminal fusion peptide region (comprised by amino acid residues 770 to 788) might be the first one to acquire the competence to bind to and insert into the membrane, whereas the region comprised by amino acids 858 to 886 (internal fusion peptide) might be fundamental for subsequent steps of the fusion process because it would become located adjacent to the transmembrane domain after the necessary rearrangements that give rise to the formation of the six-helix coiled-coil bundle [47].

Although much information has been obtained in recent years on membrane fusion, we do not know yet the processes and the mechanism behind it. Elucidating the nature of the interactions between phospholipid and membrane proteins is essential for the understanding of the structure and function of the implicated molecules, clarifying the specific roles of specific types of phospholipids in biological membranes. Based on our work [32,46,48] we have selected three specific sequences from the SARS-CoV S2 sequence (Fig. 1), i.e., $SARS_{FP}$, comprised by amino acid residues 770 to 788 and corresponding to the putative fusion peptide of the protein, $SARS_{IFP}$, comprised by amino acid residues 873 to 888 and corresponding to the suggested internal fusion peptide, and $SARS_{PTM}$, comprised by amino acid residues 1185 to 1202 and corresponding to the PTM domain of the protein. Here, we explore the monolayer penetration of these peptides, their capacity to insert into the membrane as well as the perturbation of the dipole potential of the bilayer. Moreover, we show through experiments using equimolar mixtures of these peptides that they might be involved in the merging of the viral and target cell membranes working synergistically in the native protein.

2. Materials and methods

2.1. Materials and reagents

Peptides pertaining to the S2 domain of SARS-CoV (^{770}MWKTPTLKYFGGFNFSQIL^{788}, $SARS_{FP}$), (^{873}GAALQIPFAMQMAYRF^{888}, $SARS_{IFP}$) and (^{1185}LGKYEQYIKWPWYVWLGF^{1202}, $SARS_{PTM}$) with N-terminal acetylation and C-terminal amidation were obtained from Genemed Synthesis (San Francisco, CA, USA). The $SARS_{FP}$ peptide has a Trp residue replacing a Tyr one. This conservative substitution has no effect in membrane perturbation and fusion assays as shown elsewhere [34]. The peptides were purified by reverse-phase HPLC (Vydac C-8 column, 250×4.6 mm, flow rate 1 ml/min, solvent A, 0.1% trifluoroacetic acid, solvent B, 99.9 acetonitrile and 0.1% trifluoroacetic acid) to better than 95% purity, and its composition and molecular mass were confirmed by amino acid analysis and mass spectroscopy. 1-Palmitoyl-2-oleoyl-*sn*-glycero-3-phosphocholine (POPC), 1-palmitoyl-2-oleoyl-*sn*-glycero-3-phosphoglycerol (POPG), egg sphingomyelin (ESM) and cholesterol (CHOL) were obtained from Avanti Polar Lipids (Alabaster, AL, USA). 4-(2-(6-(Dioctylamino)-2-naphthalenyl) ethenyl)-1-(3-sulfopropyl)-pyridinium inner salt (di-8-ANEPPS) was obtained from Molecular Probes (Eugene, OR, USA). All other reagents used were of analytical grade from Sigma-Aldrich (Madrid, ES, EUR). Water was deonized, twice-distilled and passed through a Milli-Q equipment (Millipore Ibérica, Madrid, ES, EUR) to a resistivity higher than 18 MΩ cm.

2.2. Preparation of large unilamellar vesicles

Aliquots containing the appropriate amount of lipid in chloroform–methanol (2:1 vol/vol) were placed in a test tube, the solvents were removed by evaporation under a stream of O_2-free nitrogen, and finally, traces of solvents were eliminated under vacuum in the dark for >3 h. The lipid films were resuspended in buffer and incubated at 25 °C with intermittent vortexing for 30 min to hydrate the samples and obtain multilamellar vesicles. The samples were frozen and thawed five times to ensure complete homogenization with occasional vortexing. Large unilamellar vesicles (LUV) with a mean diameter of 0.1 μm were prepared from multilamellar vesicles by the extrusion method [49] using polycarbonate filters with a pore size of 0.1 μm (Nuclepore Corp., Cambridge, CA, USA). The phospholipid and peptide concentration was measured by methods described previously [50,51].

2.3. Insertion of peptides into lipid monolayers

Insertion of peptides into lipid monolayers, residing on an air/water interface, was measured using magnetically stirred circular Teflon wells (Multiwell plate, subphase volume 3 mL, Kibron Inc.,

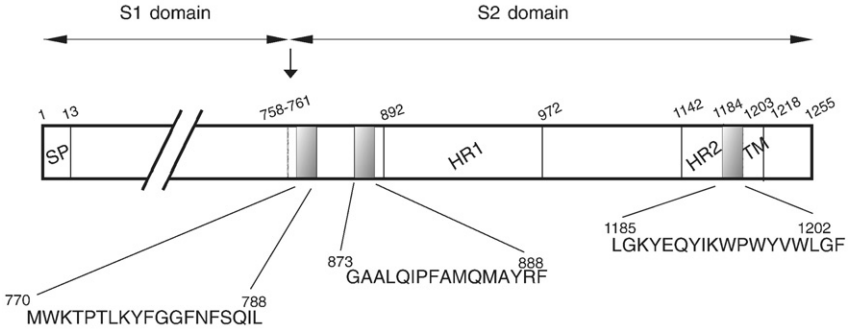

Fig. 1. Schematic view of the organization of SARS-CoV spike glycoprotein S (amino acid residues 1 to 1255 for the full length), showing the approximate structural and functional regions: the predicted heptad repeat regions HR1 and HR2, the transmembrane domain (TM) and the relative position of the peptides used in this study which correspond to the fusion peptide ($SARS_{FP}$), the internal fusion peptide ($SARS_{IFP}$) and the pre-transmembrane domain ($SARS_{PTM}$). The sequences of the peptides are also shown.

Helsinki, FIN). Surface pressure (π) was monitored with a Wilhelmy wire attached to a microbalance (DeltaPi, Kibron Inc., Helsinki, FIN, EUR) interfaced to a computer. Lipids were mixed at the indicated molar ratios in chloroform (approximately 1 mM) and then spread onto the air-buffer interface (20 mM HEPES, 0.1 mM EDTA, pH 7.4). The lipid monolayers were allowed to equilibrate for approximately 15 min at different initial surface pressures (π_0) before the injection of the peptides into the subphase. The increment in π after peptide addition was complete in approximately 30 min and the difference between the initial surface pressure (π_0) and the value observed after the penetration of peptide into the films was taken as $\Delta\pi$. The data shown represent the average from triplicate measurements and are represented as $\Delta\pi$ vs. π_0. These graphs yield the critical surface pressure π_c corresponding to the lipid lateral packing density preventing the intercalation of the peptides into the lipid films. All measurements were performed at ambient temperature (≈25 °C).

2.4. Compression isotherms

A computer-controlled Langmuir type film balance (μTrough XL, Kibron Inc., Helsinki, FIN) equipped with a Precision Plus trough was used to measure π-A isotherms, using the embedded features of the control software (FilmWare 3.57, Kibron Inc., Helsinki, FIN, EUR). The indicated lipid mixtures were made in chloroform and were spread onto the air–aqueous phase interface (20 mM HEPES, 0.1 mM EDTA, pH 7.4) with a microsyringe (Hamilton); mixtures of peptides were added prior to lipid. The total surface area of the trough was 120 cm^2 and the volume of the subphase was 35 ml. After 5 min equilibration to ensure evaporation of the solvent, the film compression was started using two symmetrically moving barriers. Compression rate was 4 $Å^2$/chain/min, to allow for the reorientation and relaxation of the lipids in the course of the compression. Surface pressure (π) was monitored with a metal alloy probe hanging from a high precision microbalance (KBN 315, Kibron Inc., Helsinki, FIN, EUR) connected to a computer. Each run was repeated at least twice to ensure reproducibility.

2.5. Quenching of Trp emission by acrylamide

Peptides were added to a solution of LUVs and after 1 h of equilibration, fluorescence emission spectra were recorded in a SLM Aminco 8000 spectrofluorometer with excitation and emission wavelengths of 290 and 343 nm, respectively, and 4 nm spectral bandwiths. Measurements were carried out in 20 mM HEPES, EDTA 0.1 mM, pH 7.4. Intensity values were corrected for dilution, and the scatter contribution was derived from lipid titration of a vesicle blank. Aliquots of a 4 M solution of the water-soluble quencher acrylamide were added to the peptide in the absence or the presence of the liposomes. The lipid-to-peptide ratio was 100:1. The values obtained were corrected for dilution, and the scatter contribution was derived from acrylamide titration of a vesicle blank. The data were analyzed according to the Stern–Volmer equation [52], $F_0/F = 1 + K_{sv}[Q]$, where F_0 and F represent the fluorescence intensities in the absence and the presence of the quencher [Q], respectively, and K_{sv} is the Stern–Volmer quenching constant.

2.6. Measurement of the membrane dipole potential

Aliquots containing the appropriate amount of lipid in chloroform–methanol (2:1 v/v) and di-8-ANEPPS were placed in a test tube to obtain a probe/lipid molar ratio of 1/100 and LUVs with a mean diameter of 0.1 μm were prepared as described previously. Steady-state fluorescence measurements were recorded with a Varian Cary Eclipse spectrofluorimeter. Dual wavelength recordings with the dye di-8-ANEPPS were obtained by exciting the samples at two different wavelengths (450 and 520 nm) and measuring their intensity ratio, R (450/520), at an emission wavelength of 620 nm [53,54]. This ratio reflects the changes in the total membrane dipole potential moment, as they cause a shift in the excitation spectrum maximum of di-8-ANEPPS. By exciting the membrane suspensions at two different wavelengths corresponding to the maximum and the minimum of the difference spectrum, a fluorescence intensity ratio R can be calculated, which can be used as a measure of the relative changes in the magnitude of the dipole potential. The fluorescence ratio R is defined as the ratio of the fluorescence intensity at an excitation wavelength of 450 nm divided by that at 520 nm. The lipid concentration was 200 μM, and all experiments were performed at room temperature.

3. Results

The SARS-CoV spike glycoprotein, classified as a Class I viral fusion protein, consists of an extracellular domain, a transmembrane domain, and an intracellular domain (Fig. 1). It is also known that several regions of viral fusion proteins bind and interact with membranes, experience conformational changes and interact between each other, which make possible the fusion of the viral and cell membranes [55,56]. From our previous work, we have selected three specific sequences from the SARS-CoV S2 sequence, i.e., $SARS_{FP}$, $SARS_{IFP}$ and $SARS_{PTM}$ (S2 regions comprising residues from 770 to 788, from 873 to 888, and from 1185 to 1202, see Fig. 1) to explore the interaction of these peptides, either alone or in combination, with monolayers or LUV_S having different lipid compositions.

3.1. Penetration of SARS S2 derived peptides into lipid monolayers

The insertion of the SARS S2 derived peptides $SARS_{FP}$, $SARS_{IFP}$ and $SARS_{PTM}$ into lipid monolayers with different initial pressures π_0 was measured by observing the increment in surface pressure ($\Delta\pi$) following the addition of the peptides into the subphase (Fig. 2 and Table 1). Interestingly, there was a different behavior of the different peptides depending on the lipid composition of the monolayers. Peptide $SARS_{PTM}$ is highly surface active and was intercalated effectively in all four different lipidic compositions (Fig. 2A). However, the overall charge of the lipid monolayer played a significant role in peptide insertion, since we observed an increase in π_c from 35 mN/m for POPC monolayers to 45 mN/m for POPC/POPG monolayers. The presence of either ESM or CHOL reduced the intercalation of the $SARS_{PTM}$ peptide, since π_c decreased to 31 and 30 mN/m, respectively in the presence of these lipids. In contrast to $SARS_{PTM}$, the increment in the surface pressure at low π_0 was different for $SARS_{FP}$ (Fig. 2B). Whereas the maximum $\Delta\pi$ varied between 25 and 31 mN/m for the $SARS_{PTM}$ peptide, the values measured for the $SARS_{FP}$ peptide varied between 15 and 21 mN/m, suggesting a more shallow location of the latter peptide. The presence of a negatively-charged phospholipid induced a similar effect as observed for $SARS_{PTM}$, π_c increasing from 32 mN/m to 41 mN/m. Similarly, the presence of either ESM or CHOL reduced π_c from 32 mN/m to about 25 mN/m (Table 1). In the case of the $SARS_{IFP}$ peptide, the maximum $\Delta\pi$ values were similar to those found for $SARS_{FP}$, but the dependence of π_c on monolayer composition was very different (Fig. 2C). Interestingly, $SARS_{IFP}$ readily intercalated into POPC monolayers with a π_c value of 40 mN/m, but the presence of POPG diminished its insertion, displaying a π_c value of approximately 26 mN/m. Interestingly, the presence of CHOL abolished completely the insertion of the $SARS_{IFP}$ peptide, since the π_c value observed was about 16 mN/m. However, the presence of both ESM and CHOL increased π_c to 29 mN/m.

3.2. Penetration of SARS S2 derived peptides mixtures into lipid monolayers

As it was commented previously, and in the context of the membrane fusion mechanism elicited by SARS-CoV envelope

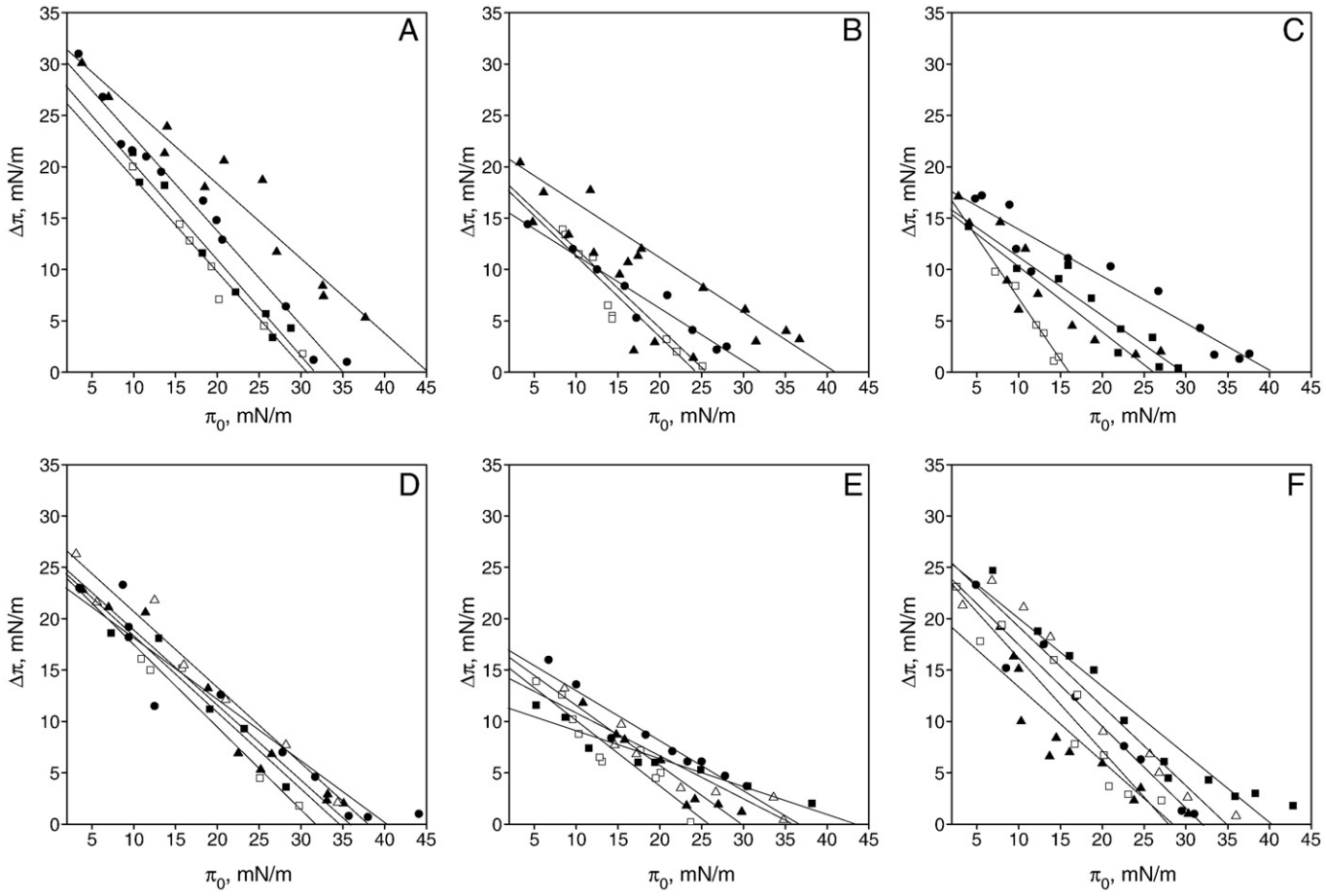

Fig. 2. Insertion into lipid monolayers of the S2 SARS-CoV derived peptides. The increment in the surface pressure ($\Delta\pi$) of the lipid monolayer due to the addition of (A) $SARS_{PTM}$, (B) $SARS_{FP}$, (C) $SARS_{IFP}$, (D) an equimolar mixture of $SARS_{FP}$ and $SARS_{PTM}$, (E) an equimolar mixture of $SARS_{IFP}$ and $SARS_{FP}$ and (F) an equimolar mixture of $SARS_{PTM}$ and $SARS_{IFP}$ into the subphase as a function of the initial pressure (π_0). The lipid compositions of the monolayers were POPC (●), POPC/POPG at a molar ratio of 7:3 (▲), POPC/ESM/CHOL at a molar ratio of 8:1:1 (■), POPC/CHOL at a molar ratio of 8:2 (□) and POPC/ESM at a molar ratio of 8:2 (Δ).

glycoprotein S, the concerted action of several membrane-interacting domains may have an essential role in facilitating it. Moreover, after the rearrangements of the protein to form the six-helix coiled-coil bundle, some of them would be adjacent to each other and therefore interact together. Consequently, we also analyzed the insertion of equimolar combinations of the three former peptides in monolayers having different compositions. The insertion of an equimolar combination of $SARS_{FP}$ plus $SARS_{PTM}$ in monolayers of different compositions is showed in Fig. 2D. As expected, the increment in surface pressure at low π_0 was centered between the maxima observed with both peptides alone. However, depending on lipid composition some differences were observed compared to the data shown above using single peptides. For POPC monolayers, π_c was 40 mN/m, in contrast with a predicted value of about 33 mN/m, when assuming an independent effect for each of the peptides (Table 1). In the case of the mixture POPC/POPG, the experimental π_c was 36 mN/m, significantly lower than the predicted one of about 43 mN/m. In the presence of mixtures containing ESM or CHOL, the π_c values were slightly decreased when compared with pure POPC (35 mN/m and 32 mN/m, respectively). The mixture containing ESM alone did yield a π_c of about 38 mN/m, i.e., in between POPC and POPC/ESM/CHOL (Table 1). The insertion into monolayers of an equimolar combination of $SARS_{FP}$ plus $SARS_{IFP}$ is shown in Fig. 2D. The π_c values in POPC and POPC/POPG monolayers were similar to the predicted ones, i.e., 36 mN/m and 30 mN/m (Table 1). The inclusion of CHOL in POPC gave place to a π_c value of 26 mN/m, greater than the predicted one. However, the inclusion of ESM in POPC did not induce any difference in π_c when compared with pure POPC. However, the inclusion of both ESM and CHOL promoted a strong increase in π_c (43 mN/m). In this case, the $\Delta\pi$ value at low π_0 was less pronounced than that observed in the other lipids suggesting a shallow penetration of the peptides in the monolayer. The insertion of an equimolar combination of $SARS_{PTM}$ plus $SARS_{IFP}$ in monolayers is showed in Fig. 2F (see Table 1). In POPC and POPC/POPG monolayers, the π_c values were lower than the predicted ones (32 mN/m and 28 mN/m, respectively). However, the presence of either ESM or CHOL to POPC gave place to π_c values significantly increased if compared with the predicted ones (40 mN/M, 28 mN/M

Table 1
Critical surface pressure π_c values for monolayers having different lipid compositions in the presence of the SARS derived peptides as indicated

Lipid composition of the monolayers	$SARS_{PTM}$	$SARS_{FP}$	$SARS_{IFP}$	$SARS_{FP}$ +$SARS_{PTM}$ (1:1)		$SARS_{FP}$ +$SARS_{IFP}$ (1:1)		$SARS_{IFP}$ +$SARS_{PTM}$ (1:1)	
	Exp[a]	Exp	Exp	Exp	Aver[b]	Exp	Aver	Exp	Aver
POPC	35	32	40	40	33.5	36	36	32	37.5
POPC/POPG (7:3)	45	41	26	36	43	30	33.5	28	35.5
POPC/ESM/CHOL (8:1:1)	31	25	29	35	28	43	27	40	30
POPC/CHOL (8:2)	30	24	16	32	27	26	20	28	23
POPC/ESM (8:2)	–	–	–	38	–	36	–	35	-

[a] Exp, experimental values obtained through the analysis of the data presented in Fig. 2.
[b] Aver, average value obtained from the sum of the individual experimental values.

and 35 mN/M for POPC/ESM/CHOL, POPC/CHOL and POPC/ESM, respectively).

3.3. Changes in the membrane potential by SARS S2 derived peptides

Changes in the membrane dipole potential elicited by SARS S2 derived peptides and their combinations were monitored by means of the spectral shift of the fluorescence probe di-8-ANEPPS [53]. The variation of the fluorescence intensity ratio $R_{450/520}$ normalized as a function of the peptide concentration for different membrane compositions is shown in Fig. 3. In the presence of the $SARS_{PTM}$ peptide a great decrease in the $R_{450/520}$ value was measured in the presence of the three mixtures tested, being slightly higher in the presence of POPC/POPG than in the POPC and POPC/ESM/CHOL samples (Fig. 3A). In contrast to the former peptide, $SARS_{IFP}$ had no significant effect on the membrane dipole potential (Fig. 3B), suggesting that this peptide, despite being inserted in monolayers, is not able to insert sufficiently in order to perturb the membrane potential, or inserts in a way causing minimal alteration in the dipole potential. For $SARS_{FP}$, the change of dipole potential is less pronounced than that caused by $SARS_{PTM}$ (Fig. 3C), suggesting a shallow position of $SARS_{FP}$ in the membrane, in accordance with the monolayer data shown above. However, the dependence on lipid composition is significantly more pronounced than seen for $SARS_{PTM}$. In the presence of membranes composed of POPC/POPG, the membrane potential underwent a strong perturbation by the peptide, whereas for pure POPC was smaller and quite insignificant in the case of POPC/ESM/CHOL (Fig. 3C).

3.4. Changes in the membrane potential by SARS S2 derived peptides mixtures

In a similar way as before, we carried out experiments with equimolar mixtures of the three peptides. The combination of $SARS_{FP}$ plus $SARS_{PTM}$ showed a change in membrane dipole potential similar to the sum of the effects produced by the peptides alone, supposing an independent and additive effect of each one of the peptides, with the exception of the POPC/ESM/CHOL sample, where the experimental value is greater than the expected linear sum (Fig. 3D). For the mixture of the $SARS_{FP}$ and $SARS_{IFP}$ peptides, a slight decrease of R is seen for all the samples (Fig. 3E). Finally, we analyzed the effect of an equimolar mixture of $SARS_{IFP}$ and $SARS_{PTM}$ on the membrane dipole potential as shown in Fig. 3F. In this case, the decrease in the R value was significant, taking into account that $SARS_{PTM}$ but not $SARS_{IFP}$ had a significant effect on the dipole potential of the different membranes tested. Therefore, a cooperative effect between $SARS_{PTM}$ and $SARS_{IFP}$ can be inferred from the data.

3.5. Quenching of SARS S2 derived peptides by acrylamide

We also studied the accessibility of the Trp residues of the peptides, either alone or in an equimolar combination, to collisional quenching by acrylamide, a neutral, water-soluble, highly efficient quencher, which is unable to penetrate into the hydrophobic core of the lipid bilayer. The quenching data are presented in Fig. 4 and the Stern–Volmer quenching constants shown in Table 2. The linear Stern–Volmer plots with a unitary intercept indicate that the Trp

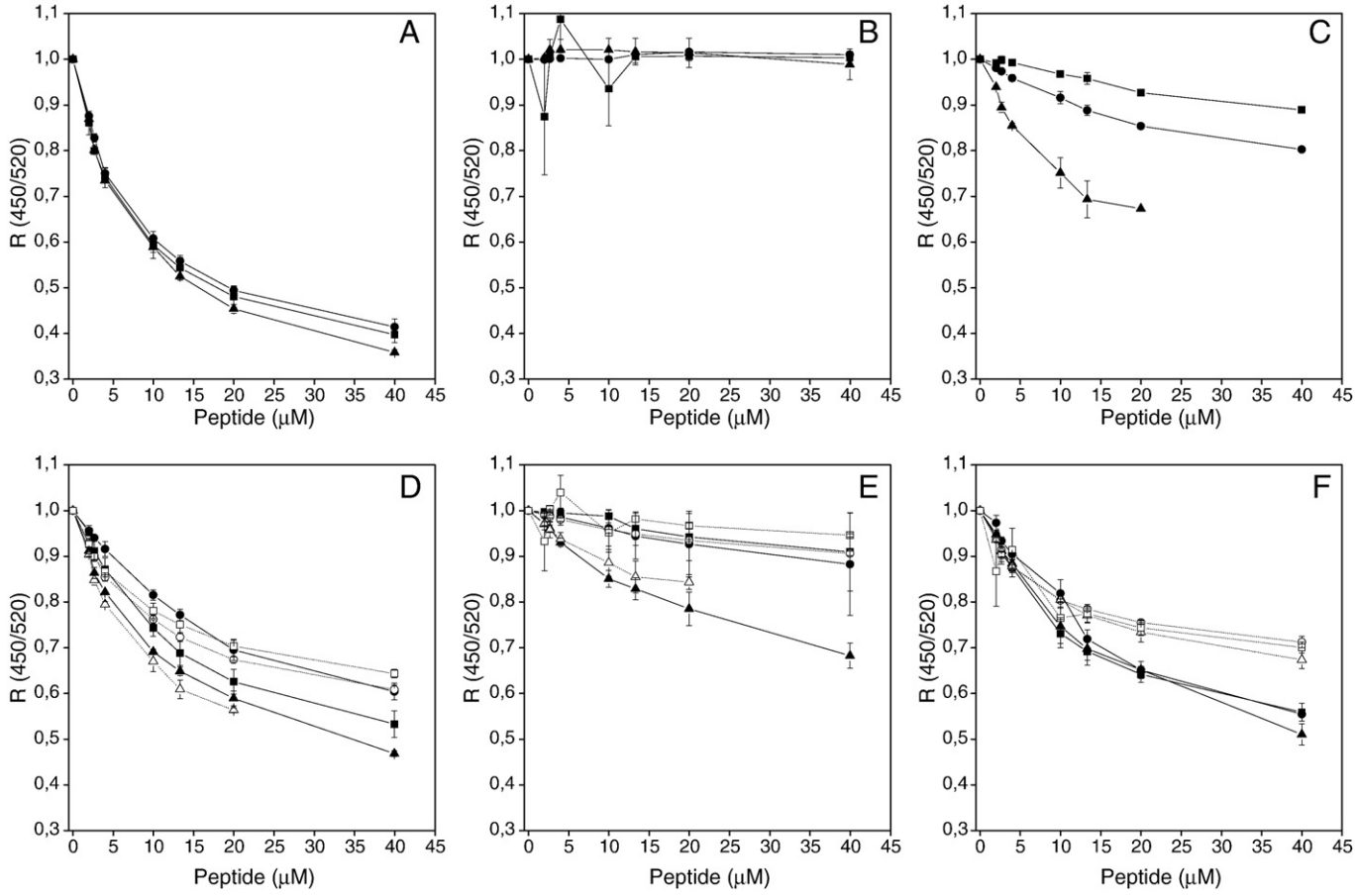

Fig. 3. Effect of (A) $SARS_{PTM}$, (B) $SARS_{IFP}$, (C) $SARS_{FP}$, (D) an equimolar mixture of $SARS_{FP}$ and $SARS_{PTM}$, (E) an equimolar mixture of $SARS_{IFP}$ and $SARS_{FP}$ and (F) an equimolar mixture of $SARS_{PTM}$ and $SARS_{IFP}$ on the membrane dipole potential monitored through the fluorescence ratio (R) of di-8ANEPPS labelled LUVs containing different lipid compositions at different lipid-to-peptide molar ratios. The lipid compositions were POPC (●), POPC/POPG at a molar ratio of 7:3 (▲) and POPC/ESM/CHOL at a molar ratio of 8:1:1 (■). Values obtained by summing the single peptide experimental values are indicated by empty symbols and dashed lines.

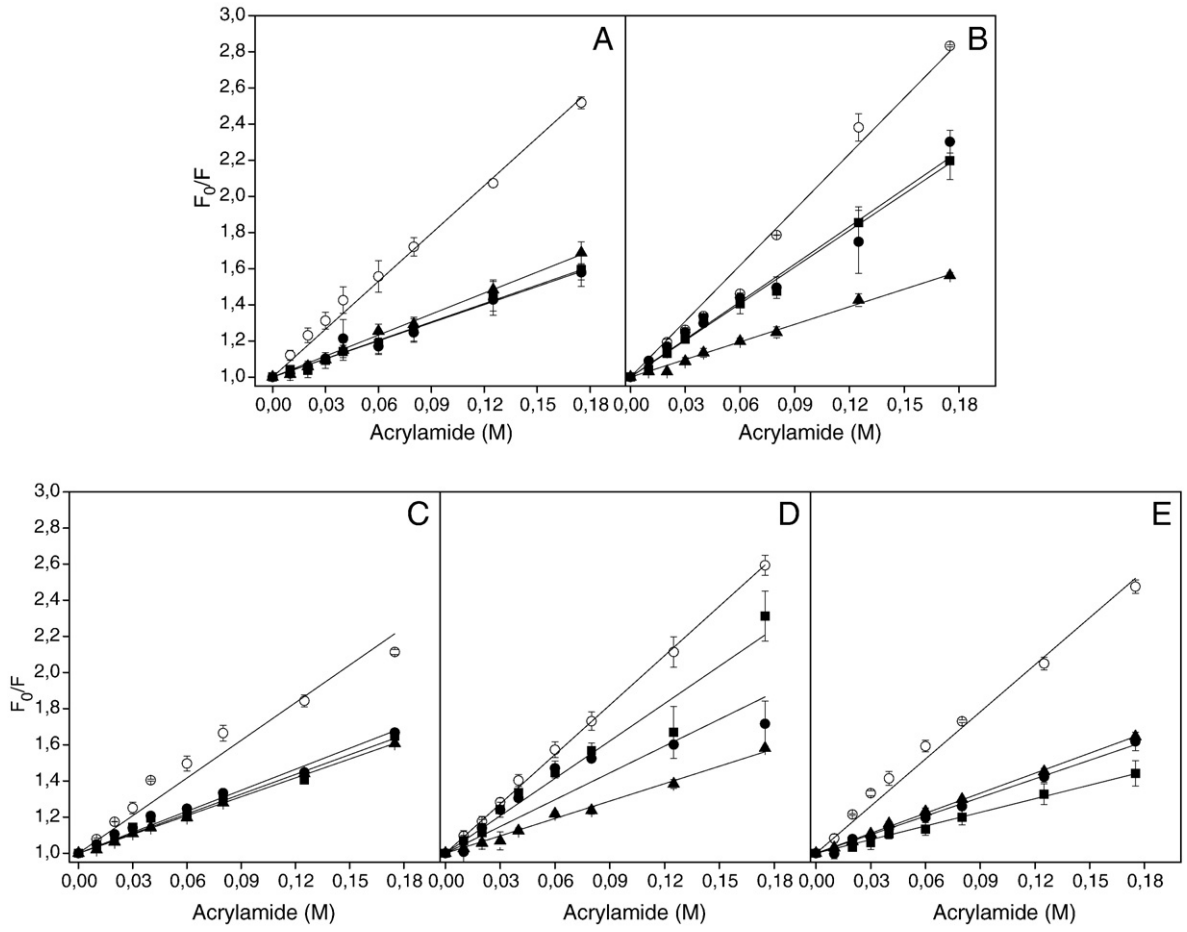

Fig. 4. Stern–Volmer plots of the quenching of the Trp fluorescence emission of (A) $SARS_{PTM}$, (B) $SARS_{FP}$, (C) an equimolar mixture of $SARS_{FP}$ and $SARS_{PTM}$, (D) an equimolar mixture of $SARS_{IFP}$ and $SARS_{FP}$ and (E) an equimolar mixture of $SARS_{PTM}$ and $SARS_{IFP}$ by acrylamide in aqueous buffer (○) and in the presence of liposomes composed of POPC (●), POPC/POPG at a molar ratio of 7:3 (▲) and POPC/ESM/CHOL at a molar ratio of 8:1:1 (■). The lipid-to-peptide ratio was 100:1. The fittings to the Stern–Volmer equation are also shown.

residues are fairly accessible to acrylamide, and in all cases, the quenching showed an acrylamide dependent concentration behavior, so that the Stern–Volmer dynamic quenching formalism describes accurately the data. It is necessary to mention here that the $SARS_{PTM}$ peptide has three Trp residues, and the $SARS_{FP}$ peptide has a Trp residue. $SARS_{IFP}$ was used in its wild type form, i.e., without Trp residues, because it is only necessary for one peptide in the mixture to obtain relevant fluorescence data. The quenching data for the $SARS_{PTM}$ peptide is presented in Fig. 4A and the resultant Stern–Volmer plots reveal that in aqueous solution the Trp residues were highly exposed to the solvent that led to a more efficient quenching. However, in the presence of model membranes, the extent of quenching was significantly reduced, indicating a poor accessibility of the Trp residues to the aqueous phase, consistent with the incorporation of the $SARS_{PTM}$ peptide into the lipid bilayer. Interestingly, the K_{SV} values were similar showing no preference for any one of the lipid compositions used (Table 2). In contrast, and in the presence of $SARS_{FP}$, different K_{SV} values were measured, being lowest for the POPC/POPG liposomes (Fig. 4B). These data indicate that the Trp of the $SARS_{FP}$ peptide is less exposed to the aqueous solvent in the presence of membranes containing negatively-charged phospholipids than the other mixtures (Table 2), in accordance with the monolayer and membrane potential experiments shown above.

3.6. Quenching of SARS S2 derived peptides mixtures by acrylamide

The Stern–Volmer plots for the quenching of Trp in samples containing equimolar mixtures of $SARS_{FP}$ and $SARS_{PTM}$ are shown in Fig. 4C. The K_{SV} values in the presence of all types of membranes were lower than in solution, indicating that the peptide mixture was effectively incorporated into the membranes, showing no preference for any one of them. Significantly, and comparing the K_{SV} values in solution (Table 2), the single peptides showed larger values than the equimolar mixture (8.8 M^{-1} and 10.2 M^{-1} for $SARS_{PTM}$ and $SARS_{FP}$, respectively, and 6.9 M^{-1} for the equimolar mixture of $SARS_{PTM}$ and $SARS_{FP}$), suggesting the existence of a direct peptide–peptide interaction in solution. For the equimolar mixture of the $SARS_{FP}$ and $SARS_{IFP}$ peptides (Fig. 4D), although lower K_{SV} values were obtained in the presence of membranes than in solution, the lowest was observed for the POPC/POPG sample (Table 2). These data would indicate that the preference of $SARS_{FP}$ for negatively-charged phospholipids would dominate in the mixture. The solution K_{SV} value of the $SARS_{FP}$ and $SARS_{IFP}$ mixture is slightly lower than that found for $SARS_{FP}$,

Table 2
Acrylamide Stern–Volmer quenching constant (K_{SV}/M^{-1}) for the SARS derived peptides in buffer and in the presence of LUVs of different compositions

LUV composition	$SARS_{PTM}$	$SARS_{FP}$	$SARS_{FP}$ + $SARS_{PTM}$ (1:1)	$SARS_{IFP}$ + ARS_{FP} (1:1)	$SARS_{IFP}$ + $SARS_{PTM}$ (1:1)
POPC	3.3	6.9	3.9	4.9	3.4
POPC/POPG (7:3)	3.9	3.2	3.5	3.2	3.7
POPC/ESM/CHOL (8:1:1)	3.4	6.8	3.6	6.9	2.5
Buffer	8.8	10.3	6.9	9.1	8.7

The lipid-to-peptide ratio was 100:1.

suggesting an interaction between the peptides but to a lesser extent than that found for the former mixture. In the case of the equimolar mixture of $SARS_{PTM}$ and $SARS_{IFP}$, the K_{SV} values obtained in the presence of POPC and POPC/POCG mixtures were similar but higher than that found for the mixture containing POPC/ESM/CHOL (Table 2). The K_{SV} value obtained for the mixture in solution was similar to that found for $SARS_{PTM}$, suggesting that there was no interaction between these two peptides.

3.7. Compression isotherms of SARS S2 derived peptide mixtures

To further explore the interaction of SARS derived peptides we recorded compression isotherms of pure POPC and a mixture of POPC/ESM/CHOL at a lipid molar ratio of 8:1:1 in the presence of equimolar mixtures of the SARS-CoV derived peptides (Fig. 5). As observed in the π-A isotherms, the presence of all the peptide combinations caused a significant increase in the molecular area of the phospholipid monolayer, indicating that the peptides are also occupying a fraction of the interface. All the three combination**s** were squeezed-out from the interface at a similar surface pressure, i.e., about 43–48 mN/m, as shown by the convergence of the lipid/peptide isotherms with the isotherm of the pure lipid sample. It can be also observed that the peptide interaction with the POPC/ESM/CHOL mixture is more efficient since they cause a larger increase of the surface area per molecule. For example, at a surface pressure of 10 mN/m, ΔA, the difference in area per molecule in the absence and in the presence of the peptides, was 24.4, 29 and 32.8Å^2 per molecule in POPC monolayers but it increased to 30.8, 38.7 and 44.4 Å^2 per lipid molecule in POPC/ESM/CHOL monolayers for the equimolar mixtures of $SARS_{IFP}$ + $SARS_{PTM}$, $SARS_{IFP}$ + $SARS_{FP}$ and $SARS_{PTM}$ + $SARS_{FP}$, respectively.

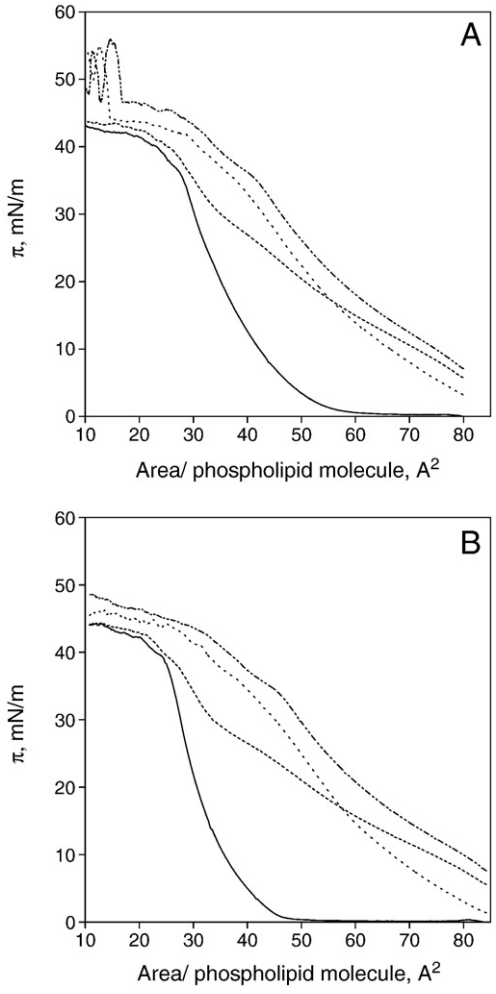

Fig. 5. Compression isotherms for monolayers composed of (A) POPC and (B) POPC/ESM/CHOL at a molar ratio of 8:1:1 in the absence (–) and in the presence of an equimolar mixture of $SARS_{FP}$ and $SARS_{PTM}$ (·–·–·), an equimolar mixture of $SARS_{IFP}$ and $SARS_{FP}$ (– – –) and an equimolar mixture of $SARS_{PTM}$ and $SARS_{IFP}$ (·····). The lipid-to-peptide ratio was approximately 5:1.

4. Discussion

Enveloped viruses use membrane fusion proteins in order to juxtapose and merge the viral and cellular membranes causing membrane fusion. The viral fusion protein of SARS-CoV is the envelope Spike glycoprotein and the domain responsible of the fusion is the S2 domain. Until recently, it has been thought that the N-terminal fusion peptide was the main region interacting with and inserting into the target cell membrane inducing fusion of the lipid bilayers. However, recent studies point to the fact that there are several regions within Class I and Class II membrane fusion proteins which are involved in the interaction with the membrane to accomplish the fusion process [20,25,26,57]. Although in other Class I fusion proteins plentiful data have been obtained to understand the implication of these membrane-interacting segments in the fusion mechanism, available information concerning the possible membrane-active regions in coronavirus, and particularly in the case of SARS-CoV, is scarce. Recent studies have identified three membranotropic regions in the S2 domain of SARS-CoV S glycoprotein, one situated downstream of the minimum furin cleavage, which is considered the fusion peptide ($SARS_{FP}$), an internal putative fusion peptide helper for the fusion peptide located immediately upstream of the HR1 region ($SARS_{IFP}$) and the pre-transmembrane domain ($SARS_{PTM}$) [32,34,45,46,48]. To test the hypothesis that these regions of the S2 protein may cooperatively interact in the native protein to create a fusion pore or destabilize the membrane, we have analyzed the monolayer insertion, change in membrane potential, peptide accessibility and compression isotherms of equimolar mixtures of the three synthetic peptides mentioned above. We report that synthetic peptides corresponding to these three membrane-interacting segments might interact with and insert into the bilayer as well as they can interact between them.

The three different peptides interact with lipid membranes depending on the lipid composition, as it is shown in the monolayer insertion and membrane dipole potential experiments. $SARS_{PTM}$ and $SARS_{FP}$ peptides insert into lipid monolayers and their intercalation is enhanced by the presence of the negatively-charged phospholipid, POPG. Moreover, inclusion of CHOL to the lipid monolayer decreases the $SARS_{FP}$ and $SARS_{PTM}$ intercalation into lipid monolayers. Nevertheless, $SARS_{PTM}$ had a different behavior to $SARS_{FP}$ decreasing the dipole membrane potential. Whereas the change in the membrane potential was nearly independent of phospholipid composition for $SARS_{PTM}$, the dependence on negatively-charged phospholipids is stronger in the $SARS_{FP}$ peptide since the decrease in the dipole potential of the membrane was more noticeable in POPG containing LUVs. Furthermore, addition of ESM and CHOL reduces even more the change in membrane potential caused by $SARS_{FP}$. $SARS_{IFP}$ has also a different behavior depending on lipid composition. $SARS_{IFP}$ penetrates more easily into POPC than into POPG and CHOL containing monolayers. However, the presence of both CHOL and ESM abolished completely the intercalation of the peptide into the monolayer. In the case of the peptide equimolar mixtures, we can observe that the presence of both ESM and CHOL, components which mimic lipidic rafts, induce a greater insertion, particularly in the case of $SARS_{PTM}$ plus $SARS_{IFP}$ and $SARS_{IFP}$ plus $SARS_{FP}$ mixtures. A similar effect is observed in the membrane dipole potential measurements. However, the cooperation of $SARS_{PTM}$ and $SARS_{IFP}$ to change the membrane potential occurs in all phospholipidic mixtures but the synergistic

effect of the other two mixtures is more marked in LUVs mimicking lipidic rafts.

Analysis of the fluorescence data is more complicated because, in this case, we were not able to detect any effect of the mixture in the membrane and it is the fluorescence of the peptide/s containing tryptophans which allow us to infer the interaction with the membrane. Despite this fact it is possible to obtain information of these experiments. For the $SARS_{PTM}$ and $SARS_{FP}$ equimolar mixture, similar low K_{SV} values were observed in the three different LUV compositions used despite the strong dependence on negative charged phospholipids observed for $SARS_{FP}$ alone. So, $SARS_{FP}$ in combination with $SARS_{PTM}$, might insert deeper into the membrane. However, it cannot be discarded that fluorescence of $SARS_{PTM}$ predominate in the mixture owing to its higher quantum yield. Lower K_{SV} values for the mixture $SARS_{PTM}$ and $SARS_{IFP}$ compared with those observed for the single peptides indicate a significant interaction between the peptides in solution. In the $SARS_{FP}$ plus $SARS_{IFP}$ mixture, the lower K_{SV} is observed in POPG, similarly to what was observed in $SARS_{FP}$ alone, so that $SARS_{IFP}$ does not seem to affect the accessibility of $SARS_{FP}$. Some type of interaction between $SARS_{FP}$ and $SARS_{IFP}$ is possible since the K_{SV} value is lower for the peptide mixture than for $SARS_{FP}$ alone, but not in the same extent that $SARS_{PTM}$ and $SARS_{IFP}$. Lastly, although the K_{SV} values for the $SARS_{PTM}$ and $SARS_{IFP}$ mixture are similar to those observed for the $SARS_{PTM}$, in the case of LUVs mimicking rafts the K_{SV} is significant lower, which would indicate a synergistic action of these peptides in order to perturb and insert into this type of membrane.

The three peptides have positive net charges, +1 for $SARS_{PTM}$ and $SARS_{IFP}$ and +2 for $SARS_{FP}$. So, it would be expected a similar influence of negatively-charged phospholipids on the membrane interaction of the peptides. However, this is not the case and different results are obtained suggesting that not only charge but hydrophobic interactions are taking place and giving place to the differences found. Taking into account the above mentioned experiments as well as previously published data [46], $SARS_{PTM}$ interaction with the membrane is not significantly dependent on the presence of negatively-charged phospholipids, in contrast to $SARS_{FP}$ [48]; however, both peptides would be embedded deeply into the membrane. $SARS_{IFP}$ is also able to bind membranes but it would be located in a shallow position at the membrane surface, perhaps prevented from inserting by the presence of negatively-charged phospholipids. Moreover, we have shown the existence of direct peptide–peptide interactions in solution between the $SARS_{PTM}$ and $SARS_{FP}$ peptides. Although it should be taken into account that the synergism we have found might be different in the intact protein or might even not exist, the experimental data described in this work would point to a possible interaction in the pre-fusion state, as it has been already shown in the case of HIV [58,59]. In this last case, it has been reported the formation of a complex between similar domains in the gp41 pre-fusion state acting as a kinetic trap to halt fusion. There is also ample data suggesting that in the case of HIV membrane fusion starts before the collapse of the six-helix bundle [60]. The mechanism of SARS seems to be similar in some aspects and it might behave in the same way. In Fig. 6 we present a hypothetical model of SARS-CoV fusion based on available data [32,34,45–47]. In this model, the FP would insert into the host cell, it would be followed by the formation of the pre-hairpin intermediate, and afterwards the core formed by the HR1 and HR2 would be refolded into the six-helix bundle. Subsequently hemifusion would be induced, this process being facilitated by the juxtaposition of the IFP and PTM domains. These two regions could also facilitate the formation of the fusion pore through lipid destabilization in the late steps of the membrane fusion process. The interaction between the IFP and the PTM would be one of the most important steps of this process.

It has been suggested that other class I fusion proteins might utilize similar motifs to hide and control the membrane-active

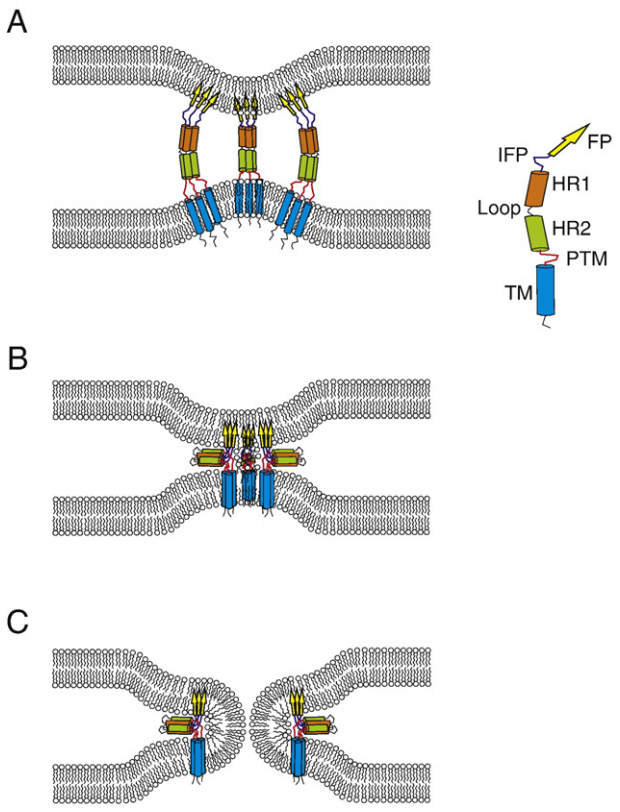

Fig. 6. Hypothetical model of SARS-CoV fusion based on available data [32,34,45–47]. (A) The FP (yellow) inserts into the host cell, it is followed by the formation of the pre-hairpin intermediate, and the core formed by the HR1 (orange) and HR2 (green) is refolded into the six-helix bundle. (B) Subsequently hemifusion is induced, this process being facilitated by the juxtaposition of the IFP (blue) and PTM (red) domains. These two regions could also facilitate the formation of the fusion pore through lipid destabilization in the late steps of the membrane fusion process, (C) leading to the complete fusion.

sequences within metastable structures. In this way, in SARS-CoV, $SARS_{PTM}$ and $SARS_{FP}$ might be forming a complex in the pre-fusion state: just after exposing the fusion peptide and its insertion into the host membrane, the formation of the six-helix bundle would bring into close proximity the region immediately upstream of HR1 ($SARS_{IFP}$) and the pre-transmembrane domain ($SARS_{PTM}$). They would find the appropriate platform in the existent lipid rafts to facilitate their interaction, and therefore facilitating the membrane fusion process. Lipid rafts are functional membrane microdomains where sphingolipids, cholesterol and associated proteins are enriched. They have been shown to play a crucial role in many biological events requiring the integrity of raft microdomains [61,62]. In addition, many viruses often use lipid rafts as a site for entry, assembly and budding. Lipid rafts have been reported to be implicated in the entry process of HIV [63], Semliki Forest virus [64] and simian virus 40 [65]. In the case of coronavirus, there also some evidence that lipid rafts are involved in virus entry [66,67]. Recent studies have reported that lipid rafts are involved in SARS-CoV entry into cells, although it is not clear if ACE2 directly localize in rafts or not. Therefore, it has been proposed that some unknown factors involved in virus entry may localize to lipid rafts [7]. In the present work, we have showed that some regions of the SARS-CoV S2 glycoprotein, mainly $SARS_{PTM}$ and $SARS_{IFP}$, can have a different interaction with lipid rafts. Consequently, lipid rafts might serve as a platform for several regions in native spike glycoprotein to interact and facilitate the membrane fusion process. In this way, lipid rafts induce and modulate the joining of components of the membrane

docking and fusion machinery making possible their intermolecular interactions by proximity [68,69].

Acknowledgements

This work was supported by grant BFU2005-00186-BMC (Ministerio de Ciencia y Tecnología, Spain) to JV. JG is recipient of predoctoral fellowship from the Autonomous Government of the Valencian Community, Spain. We are especially grateful to FEBS for a short-term fellowship to JG. The assistance by Dr. K. Sabatini in the monolayer experiments is acknowledged. HBBG is supported by the Academy of Finland and the Sigrid Jusélius Foundation (PKJK).

References

[1] M.A. Marra, S.J. Jones, C.R. Astell, R.A. Holt, A. Brooks-Wilson, Y.S. Butterfield, J. Khattra, J.K. Asano, S.A. Barber, S.Y. Chan, A. Cloutier, S.M. Coughlin, D. Freeman, N. Girn, O.L. Griffith, S.R. Leach, M. Mayo, H. McDonald, S.B. Montgomery, P.K. Pandoh, A.S. Petrescu, A.G. Robertson, J.E. Schein, A. Siddiqui, D.E. Smailus, J.M. Stott, G.S. Yang, F. Plummer, A. Andonov, H. Artsob, N. Bastien, K. Bernard, T.F. Booth, D. Bowness, M. Czub, M. Drebot, L. Fernando, R. Flick, M. Garbutt, M. Gray, A. Grolla, S. Jones, H. Feldmann, A. Meyers, A. Kabani, Y. Li, S. Normand, U. Stroher, G.A. Tipples, S. Tyler, R. Vogrig, D. Ward, B. Watson, R.C. Brunham, M. Krajden, M. Petric, D.M. Skowronski, C. Upton, R.L. Roper, The genome sequence of the SARS-associated coronavirus, Science 300 (2003) 1399–1404.

[2] P.A. Rota, M.S. Oberste, S.S. Monroe, W.A. Nix, R. Campagnoli, J.P. Icenogle, S. Penaranda, B. Bankamp, K. Maher, M.H. Chen, S. Tong, A. Tamin, L. Lowe, M. Frace, J.L. DeRisi, Q. Chen, D. Wang, D.D. Erdman, T.C. Peret, C. Burns, T.G. Ksiazek, P.E. Rollin, A. Sanchez, S. Liffick, B. Holloway, J. Limor, K. McCaustland, M. Olsen-Rasmussen, R. Fouchier, S. Gunther, A.D. Osterhaus, C. Drosten, M.A. Pallansch, L.J. Anderson, W.J. Bellini, Characterization of a novel coronavirus associated with severe acute respiratory syndrome, Science 300 (2003) 1394–1399.

[3] S. Riley, C. Fraser, C.A. Donnelly, A.C. Ghani, L.J. Abu-Raddad, A.J. Hedley, G.M. Leung, L.M. Ho, T.H. Lam, T.Q. Thach, P. Chau, K.P. Chan, S.V. Lo, P.Y. Leung, T. Tsang, W. Ho, K.H. Lee, E.M. Lau, N.M. Ferguson, R.M. Anderson, Transmission dynamics of the etiological agent of SARS in Hong Kong: impact of public health interventions, Science 300 (2003) 1961–1966.

[4] B. Kan, M. Wang, H. Jing, H. Xu, X. Jiang, M. Yan, W. Liang, H. Zheng, K. Wan, Q. Liu, B. Cui, Y. Xu, E. Zhang, H. Wang, J. Ye, G. Li, M. Li, Z. Cui, X. Qi, K. Chen, L. Du, K. Gao, Y.T. Zhao, X.Z. Zou, Y.J. Feng, Y.F. Gao, R. Hai, D. Yu, Y. Guan, J. Xu, Molecular evolution analysis and geographic investigation of severe acute respiratory syndrome coronavirus-like virus in palm civets at an animal market and on farms, J. Virol. 79 (2005) 11892–11900.

[5] Z. Qinfen, C. Jinming, H. Xiaojun, Z. Huanying, H. Jicheng, F. Ling, L. Kunpeng, Z. Jingqiang, The life cycle of SARS coronavirus in Vero E6 cells, J. Med. Virol. 73 (2004) 332–337.

[6] G. Simmons, J.D. Reeves, A.J. Rennekamp, S.M. Amberg, A.J. Piefer, P. Bates, Characterization of severe acute respiratory syndrome-associated coronavirus (SARS-CoV) spike glycoprotein-mediated viral entry, Proc. Natl. Acad. Sci. U. S. A. 101 (2004) 4240–4245.

[7] H. Wang, P. Yang, K. Liu, F. Guo, Y. Zhang, G. Zhang, C. Jiang, SARS coronavirus entry into host cells through a novel clathrin- and caveolae-independent endocytic pathway, Cell Res. 18 (2008) 290–301.

[8] X. Xiao, S. Chakraborti, A.S. Dimitrov, K. Gramatikoff, D.S. Dimitrov, The SARS-CoV S glycoprotein: expression and functional characterization, Biochem. Biophys. Res. Commun. 312 (2003) 1159–1164.

[9] M.W. Howard, B. Tripet, M.G. Jobling, R.K. Holmes, K.V. Holmes, R.S. Hodges, Dissection of the fusion machine of SARS-coronavirus, Adv. Exp. Med. Biol. 581 (2006) 319–322.

[10] Y. Xu, J. Zhu, Y. Liu, Z. Lou, F. Yuan, Y. Liu, D.K. Cole, L. Ni, N. Su, L. Qin, X. Li, Z. Bai, J.I. Bell, H. Pang, P. Tien, G.F. Gao, Z. Rao, Characterization of the heptad repeat regions, HR1 and HR2, and design of a fusion core structure model of the spike protein from severe acute respiratory syndrome (SARS) coronavirus, Biochemistry 43 (2004) 14064–14071.

[11] P. Ingallinella, E. Bianchi, M. Finotto, G. Cantoni, D.M. Eckert, V.M. Supekar, C. Bruckmann, A. Carfi, A. Pessi, Structural characterization of the fusion-active complex of severe acute respiratory syndrome (SARS) coronavirus, Proc. Natl. Acad. Sci. U. S. A. 101 (2004) 8709–8714.

[12] W.R. Gallaher, Similar structural models of the transmembrane proteins of Ebola and avian sarcoma viruses, Cell 85 (1996) 477–478.

[13] P. Chambers, C.R. Pringle, A.J. Easton, Heptad repeat sequences are located adjacent to hydrophobic regions in several types of virus fusion glycoproteins, J. Gen. Virol. 71 (Pt 12) (1990) 3075–3080.

[14] B.J. Bosch, B.E. Martina, R. Van Der Zee, J. Lepault, B.J. Haijema, C. Versluis, A.J. Heck, R. De Groot, A.D. Osterhaus, P.J. Rottier, Severe acute respiratory syndrome coronavirus (SARS-CoV) infection inhibition using spike protein heptad repeat-derived peptides, Proc. Natl. Acad. Sci. U. S. A. 101 (2004) 8455–8460.

[15] B. Tripet, M.W. Howard, M. Jobling, R.K. Holmes, K.V. Holmes, R.S. Hodges, Structural characterization of the SARS-coronavirus spike S fusion protein core, J. Biol. Chem. 279 (2004) 20836–20849.

[16] J. Zhu, G. Xiao, Y. Xu, F. Yuan, C. Zheng, Y. Liu, H. Yan, D.K. Cole, J.I. Bell, Z. Rao, P. Tien, G.F. Gao, Following the rule: formation of the 6-helix bundle of the fusion core from severe acute respiratory syndrome coronavirus spike protein and identification of potent peptide inhibitors, Biochem. Biophys. Res. Commun. 319 (2004) 283–288.

[17] S. Liu, G. Xiao, Y. Chen, Y. He, J. Niu, C.R. Escalante, H. Xiong, J. Farmar, A.K. Debnath, P. Tien, S. Jiang, Interaction between heptad repeat 1 and 2 regions in spike protein of SARS-associated coronavirus: implications for virus fusogenic mechanism and identification of fusion inhibitors, Lancet 363 (2004) 938–947.

[18] M.R. Moreno, R. Pascual, J. Villalain, Identification of membrane-active regions of the HIV-1 envelope glycoprotein gp41 using a 15-mer gp41-peptide scan, Biochim. Biophys. Acta 1661 (2004) 97–105.

[19] A.J. Perez-Berna, M.R. Moreno, J. Guillen, A. Bernabeu, J. Villalain, The membrane-active regions of the hepatitis C virus E1 and E2 envelope glycoproteins, Biochemistry 45 (2006) 3755–3768.

[20] S.G. Peisajovich, O. Samuel, Y. Shai, Paramyxovirus F1 protein has two fusion peptides: implications for the mechanism of membrane fusion, J. Mol. Biol. 296 (2000) 1353–1365.

[21] S.G. Peisajovich, R.F. Epand, M. Pritsker, Y. Shai, R.M. Epand, The polar region consecutive to the HIV fusion peptide participates in membrane fusion, Biochemistry 39 (2000) 1826–1833.

[22] R. Pascual, M.R. Moreno, J. Villalain, A peptide pertaining to the loop segment of human immunodeficiency virus gp41 binds and interacts with model bio-membranes: implications for the fusion mechanism, J. Virol. 79 (2005) 5142–5152.

[23] S. Galdiero, A. Falanga, M. Vitiello, H. Browne, C. Pedone, M. Galdiero, Fusogenic domains in herpes simplex virus type 1 glycoprotein H, J. Biol. Chem. 280 (2005) 28632–28643.

[24] T. Suarez, W.R. Gallaher, A. Agirre, F.M. Goni, J.L. Nieva, Membrane interface-interacting sequences within the ectodomain of the human immunodeficiency virus type 1 envelope glycoprotein: putative role during viral fusion, J. Virol. 74 (2000) 8038–8047.

[25] M.R. Moreno, M. Giudici, J. Villalain, The membranotropic regions of the endo and ecto domains of HIV gp41 envelope glycoprotein, Biochim. Biophys. Acta 1758 (2006) 111–123.

[26] M.R. Moreno, J. Guillen, A.J. Perez-Berna, D. Amoros, A.I. Gomez, A. Bernabeu, J. Villalain, Characterization of the interaction of two peptides from the N terminus of the NHR domain of HIV-1 gp41 with phospholipid membranes, Biochemistry 46 (2007) 10572–10584.

[27] Y.G. Yu, D.S. King, Y.K. Shin, Insertion of a coiled-coil peptide from influenza virus hemagglutinin into membranes, Science 266 (1994) 274–276.

[28] R.F. Epand, J.C. Macosko, C.J. Russell, Y.K. Shin, R.M. Epand, The ectodomain of HA2 of influenza virus promotes rapid pH dependent membrane fusion, J. Mol. Biol. 286 (1999) 489–503.

[29] J.K. Ghosh, S.G. Peisajovich, M. Ovadia, Y. Shai, Structure–function study of a heptad repeat positioned near the transmembrane domain of Sendai virus fusion protein which blocks virus–cell fusion, J. Biol. Chem. 273 (1998) 27182–27190.

[30] I. Ben-Efraim, Y. Kliger, C. Hermesh, Y. Shai, Membrane-induced step in the activation of Sendai virus fusion protein, J. Mol. Biol. 285 (1999) 609–625.

[31] O. Samuel, Y. Shai, Participation of two fusion peptides in measles virus-induced membrane fusion: emerging similarity with other paramyxoviruses, Biochemistry 40 (2001) 1340–1349.

[32] J. Guillen, A.J. Perez-Berna, M.R. Moreno, J. Villalain, Identification of the membrane-active regions of the severe acute respiratory syndrome coronavirus spike membrane glycoprotein using a 16/18-mer peptide scan: implications for the viral fusion mechanism, J. Virol. 79 (2005) 1743–1752.

[33] C.M. Petit, J.M. Melancon, V.N. Chouljenko, R. Colgrove, M. Farzan, D.M. Knipe, K.G. Kousoulas, Genetic analysis of the SARS-coronavirus spike glycoprotein functional domains involved in cell-surface expression and cell-to-cell fusion, Virology 341 (2005) 215–230.

[34] B. Sainz, Jr., J.M. Rausch, W.R. Gallaher, R.F. Garry, W.C. Wimley, Identification and characterization of the putative fusion peptide of the severe acute respiratory syndrome-associated coronavirus spike protein, J. Virol. 79 (2005) 7195–7206.

[35] T. Suarez, S. Nir, F.M. Goni, A. Saez-Cirion, J.L. Nieva, The pre-transmembrane region of the human immunodeficiency virus type-1 glycoprotein: a novel fusogenic sequence, FEBS. Lett. 477 (2000) 145–149.

[36] A. Saez-Cirion, M.J. Gomara, A. Agirre, J.L. Nieva, Pre-transmembrane sequence of Ebola glycoprotein. Interfacial hydrophobicity distribution and interaction with membranes, FEBS. Lett. 533 (2003) 47–53.

[37] S. Giannecchini, A. Di Fenza, A.M. D'Ursi, D. Matteucci, P. Rovero, M. Bendinelli, Antiviral activity and conformational features of an octapeptide derived from the membrane-proximal ectodomain of the feline immunodeficiency virus trans-membrane glycoprotein, J. Virol. 77 (2003) 3724–3733.

[38] S. Galdiero, A. Falanga, M. Vitiello, M. D'Isanto, C. Collins, V. Orrei, H. Browne, C. Pedone, M. Galdiero, Evidence for a role of the membrane-proximal region of herpes simplex virus Type 1 glycoprotein H in membrane fusion and virus inhibition, Chembiochem. 8 (2007) 885–895.

[39] C.S. Robison, M.A. Whitt, The membrane-proximal stem region of vesicular stomatitis virus G protein confers efficient virus assembly, J. Virol. 74 (2000) 2239–2246.

[40] I. Munoz-Barroso, K. Salzwedel, E. Hunter, R. Blumenthal, Role of the membrane-proximal domain in the initial stages of human immunodeficiency virus type 1 envelope glycoprotein-mediated membrane fusion, J. Virol. 73 (1999) 6089–6092.

[41] K. Salzwedel, J.T. West, E. Hunter, A conserved tryptophan-rich motif in the membrane-proximal region of the human immunodeficiency virus type 1 gp41 ectodomain is important for Env-mediated fusion and virus infectivity, J. Virol. 73 (1999) 2469–2480.

[42] S. Giannecchini, M. Pistello, B. Del Santo, P. Rovero, O. Sichi, M. Bendinelli, Changes in the SU can modulate the susceptibility of feline immunodeficiency virus to TM-derived entry inhibitors, New Microbiol. 27 (2004) 77–84.

[43] M. Lorizate, N. Huarte, A. Saez-Cirion, J.L. Nieva, Interfacial pre-transmembrane domains in viral proteins promoting membrane fusion and fission, Biochim. Biophys. Acta (2008).
[44] R. Broer, B. Boson, W. Spaan, F.L. Cosset, J. Corver, Important role for the transmembrane domain of severe acute respiratory syndrome coronavirus spike protein during entry, J. Virol. 80 (2006) 1302–1310.
[45] B. Sainz, Jr., J.M. Rausch, W.R. Gallaher, R.F. Garry, W.C. Wimley, The aromatic domain of the coronavirus class I viral fusion protein induces membrane permeabilization: putative role during viral entry, Biochemistry 44 (2005) 947–958.
[46] J. Guillen, M.R. Moreno, A.J. Perez-Berna, A. Bernabeu, J. Villalain, Interaction of a peptide from the pre-transmembrane domain of the severe acute respiratory syndrome coronavirus spike protein with phospholipid membranes, J. Phys. Chem. B. 111 (2007) 13714–13725.
[47] V.M. Supekar, C. Bruckmann, P. Ingallinella, E. Bianchi, A. Pessi, A. Carfi, Structure of a proteolytically resistant core from the severe acute respiratory syndrome coronavirus S2 fusion protein, Proc. Natl. Acad. Sci. U. S. A. 101 (2004) 17958–17963.
[48] J. Guillen, R.F. Almeida, M. Prieto, J. Villalain, Structural and dynamic characterization of the interaction of the putative fusion peptide of the S2 SARS-CoV virus protein with lipid membranes, J. Phys. Chem. B. (2008).
[49] L.D. Mayer, M.J. Hope, P.R. Cullis, Vesicles of variable sizes produced by a rapid extrusion procedure, Biochim. Biophys. Acta 858 (1986) 161–168.
[50] C.S.F. Böttcher, C.M. Van Gent, C. Fries, A rapid and sensitive sub-micro phosphorus determination. Anal. Chim. Acta 1061 (1961) 203–204.
[51] H. Edelhoch, Spectroscopic determination of tryptophan and tyrosine in proteins, Biochemistry 6 (1967) 1948–1954.
[52] M.R. Eftink, C.A. Ghiron, Exposure of tryptophanyl residues in proteins. Quantitative determination by fluorescence quenching studies, Biochemistry 15 (1976) 672–680.
[53] J. Cladera, P. O'Shea, Intramembrane molecular dipoles affect the membrane insertion and folding of a model amphiphilic peptide, Biophys. J. 74 (1998) 2434–2442.
[54] E. Gross, R.S. Bedlack, Jr., L.M. Loew, Dual-wavelength ratiometric fluorescence measurement of the membrane dipole potential, Biophys. J. 67 (1994) 208–216.
[55] R.M. Epand, Fusion peptides and the mechanism of viral fusion, Biochim. Biophys. Acta 1614 (2003) 116–121.
[56] S.G. Peisajovich, Y. Shai, Viral fusion proteins: multiple regions contribute to membrane fusion, Biochim. Biophys. Acta 1614 (2003) 122–129.
[57] S.G. Peisajovich, R.F. Epand, R.M. Epand, Y. Shai, Sendai virus N-terminal fusion peptide consists of two similar repeats, both of which contribute to membrane fusion, Eur. J. Biochem. 269 (2002) 4342–4350.
[58] M. Lorizate, M.J. Gomara, B.G. de la Torre, D. Andreu, J.L. Nieva, Membrane-transferring sequences of the HIV-1 Gp41 ectodomain assemble into an immunogenic complex, J. Mol. Biol. 360 (2006) 45–55.
[59] M. Lorizate, I. de la Arada, N. Huarte, S. Sanchez-Martinez, B.G. de la Torre, D. Andreu, J.L. Arrondo, J.L. Nieva, Structural analysis and assembly of the HIV-1 Gp41 amino-terminal fusion peptide and the pretransmembrane amphipathic-at-interface sequence, Biochemistry 45 (2006) 14337–14346.
[60] R.M. Markosyan, F.S. Cohen, G.B. Melikyan, HIV-1 envelope proteins complete their folding into six-helix bundles immediately after fusion pore formation, Mol. Biol. Cell 14 (2003) 926–938.
[61] F.C. Bender, J.C. Whitbeck, M. Ponce de Leon, H. Lou, R.J. Eisenberg, G.H. Cohen, Specific association of glycoprotein B with lipid rafts during herpes simplex virus entry, J. Virol. 77 (2003) 9542–9552.
[62] K. Simons, E. Ikonen, Functional rafts in cell membranes, Nature 387 (1997) 569–572.
[63] W. Popik, T.M. Alce, CD4 receptor localized to non-raft membrane microdomains supports HIV-1 entry. Identification of a novel raft localization marker in CD4, J. Biol. Chem. 279 (2004) 704–712.
[64] A. Ahn, D.L. Gibbons, M. Kielian, The fusion peptide of Semliki Forest virus associates with sterol-rich membrane domains, J. Virol. 76 (2002) 3267–3275.
[65] L. Pelkmans, J. Kartenbeck, A. Helenius, Caveolar endocytosis of simian virus 40 reveals a new two-step vesicular-transport pathway to the ER, Nat. Cell Biol. 3 (2001) 473–483.
[66] F. Nomura, T. Inaba, S. Ishikawa, M. Nagata, S. Takahashi, H. Hotani, K. Takiguchi, Microscopic observations reveal that fusogenic peptides induce liposome shrinkage prior to membrane fusion, Proc. Natl. Acad. Sci. U. S. A. 101 (2004) 3420–3425.
[67] K.S. Choi, H. Aizaki, M.M. Lai, Murine coronavirus requires lipid rafts for virus entry and cell–cell fusion but not for virus release, J. Virol. 79 (2005) 9862–9871.
[68] T. Lang, D. Bruns, D. Wenzel, D. Riedel, P. Holroyd, C. Thiele, R. Jahn, SNAREs are concentrated in cholesterol-dependent clusters that define docking and fusion sites for exocytosis, Embo. J. 20 (2001) 2202–2213.
[69] D.V. Nicolau, Jr., K. Burrage, R.G. Parton, J.F. Hancock, Identifying optimal lipid raft characteristics required to promote nanoscale protein–protein interactions on the plasma membrane, Mol. Cell Biol. 26 (2006) 313–323.